Sensitivity Experiments of Direct Radiative Forcing Caused by Mineral Dust Simulated with a Chemical Transport Model

Teruo AOKI, Taichu Y. TANAKA, Akihiro UCHIYAMA, Masaru CHIBA, Masao MIKAMI

Meteorological Research Institute, Tsukuba, Japan

Sadayo YABUKI

The Institute of Physical and Chemical Research (RIKEN), Wako, Japan

and

Jeffrey R. KEY

NOAA/NESDIS, Madison, Wisconsin, U.S.A.

(Manuscript received 22 September 2004, in final form 1 February, 2005)

Abstract

Sensitivity experiments of direct radiative forcing (RF) caused by mineral dust (MD) for the optical and physical properties of MD, surface albedo, solar zenith angle, and cloud cover were conducted using the Streamer-based Radiative Transfer Model for ADEC Sciences (SRTMAS). The atmospheric and dust profiles were simulated with a chemical transport model at four locations: the sea off Japan, the desert in Tarim Basin, the Sahara Desert, and snow in Siberia. The optimum calculation condition to estimate RF was also tested for the effect of the number of streams used in SRTMAS on the accuracy of RF by MD and the influence of all aerosols other than MD on RF by MD or all aerosols. When several types of aerosols are contained in the atmosphere, the test results showed that the RF by MD should not be calculated from the difference in net radiation between MD-only case and an aerosol-free case, but the difference in net radiation between a case containing all aerosols and a case containing all aerosols except MD. The experiment results by this method confirmed that the sensitivity of instantaneous RF in the shortwave (SW) region at the top of the atmosphere (TOA) to the refractive index strongly depends on surface albedo. Namely, the effect of the difference in the MD model on instantaneous RF is significant over high albedo surfaces and is relatively small over the sea. This is because the multiple reflection between the atmosphere (dust) and surface enhances light absorption by dust particles over high albedo surfaces. Over desert surfaces, the instantaneous RF in SW at TOA produced both positive and negative values within the possible refractive index range of MD. The diurnally averaged RF in SW at TOA also produced both positive and negative values in the possible range of desert albedo. The effect of the spectral distribution of surface albedo on RFs in SW for the TOA, surface, and atmosphere was examined for various surfaces. It was found that for small dust particles with an effective radius of less than 0.6 μm, RFs by MD changed depending on the difference in surface type even if the broadband albedo was the

Corresponding author: Teruo Aoki, Meterological Research Institute, 1-1 Nagamine, Tsukuba, Ibaraki 305-0052, Japan
E-mail: teaoki@mri-jma.go.jp

same. This is due to the contrast of spectral distribution between albedo and the extinction coefficient of MD. The vertical positional relationship of cloud cover to dust layer was also very important for RF at TOA in all spectral regions over desert and sea surfaces. However, the effect of cloud cover was generally small over snow surface because cloud albedo was close to the underlying snow albedo.

1. Introduction

Mineral dust has a large impact on global and regional climate conditions, yet there are still large uncertainties in its optical and physical properties. According to the report of the Intergovernmental Panel on Climate Impact (IPCC; 2001), global annual mean direct radiative forcing by MD at the tropopause due to anthropogenic activities ranges from -0.6 to $+0.4$ W m^{-2} only with error bar, and the scientific understanding is also very low. This large uncertainty is due to the lack of knowledge of the optical properties (Sokolik and Toon 1999; Myhre et al. 2003) and the limited data on dust distribution (Sokolik et al. 2001). MD has the effects of scattering and absorption in the shortwave spectral region (SW), and absorption and emission in the longwave spectral (LW) region. Since the effects in SW generally exceed those in LW, MD cools the surface and heats the atmosphere. At the top of the atmosphere (TOA), RF by MD is generally positive over high albedo surfaces and negative over low albedo surfaces under clear sky conditions (Sokolik and Toon 1996; Liao and Seinfeld 1998); it also has a heating effect in the case of a dust layer lying above cloud cover (Liao and Seinfeld 1998; Takemura et al. 2002). However, over land, the sign of RF can be changed by a small difference in the optical properties of MD. Recently, it has been reported that the effect of MD mixing with anthropogenic aerosols or those from biomass burning is an increase in its absorption (Kinne and Pueschel 2001; Chou et al. 2003; Li et al. 2004), which also makes its optical properties uncertain.

The important parameters in the optical properties of MD are optical thickness, size distribution, single-scattering albedo, and asymmetry factor (or scattering phase function). Of these, single-scattering albedo is a primary factor in determining whether RF by MD is positive or negative in the atmosphere. Hansen et al. (1997) reported that the critical value of single-scattering albedo at which the aerosol impact on global mean surface temperature shifts from cooling to heating is 0.86 for fixed clouds and increases to about 0.91 when the indirect aerosol effect on clouds is included. Single-scattering albedo depends on the complex refractive index and size distribution of aerosols, and the former varies depending on the wavelength. Since these values vary with time and space, single-scattering albedo contains large uncertainties. The estimated values of single-scattering albedo from satellite, airborne- and ground-based measurements thus lie within a wide range.

Some MD models have already been proposed. The imaginary part of the refractive index and single-scattering albedo calculated in one assumed condition is 0.008 (single-scattering albedo: 0.653) at $\lambda = 0.55$ μm for the Dust-Like model (Shettle and Fenn 1979; WMO 1983) and 0.0056 (0.888) at $\lambda = 0.55$ μm for the Desert Model in the Optical Parameters of Aerosols and Clouds (OPAC) database by Hess et al. (1998). Sokolik and Golitsyn (1993) reviewed that the imaginary part of the MD refractive index ranges from 0.003 to 0.009 at $\lambda = 0.5$ μm and that the corresponding single-scattering albedos are 0.85 and 0.75 when the particle radius is 0.6 μm. Woodward (2001) made a wide spectral range refractive index dataset from the existing data, including refractive indices mentioned above, where the imaginary part of the refractive index is 0.0057 at $\lambda = 0.5$ μm. Recently, the following high values of single-scattering albedo were reported for Saharan dust: 0.97 ± 0.02 at $\lambda = 0.64$ μm from ground and satellite measurements (Kaufman et al. 2001); 0.94 at $\lambda = 0.55$ μm, a revised value by Haywood et al. (2003) from the previous measurement by Haywood et al. (2001); 0.97 ± 0.02 on average at $\lambda = 0.55$ μm from airborne measurements (Haywood et al. 2003); and 0.86 ± 0.04 for low-dust months and 0.95 ± 0.04 for high-dust months from satellite measurements (Li et al. 2004). In these estimations, relatively low values can be partly explained as an influence of biomass

burning aerosols. The corresponding imaginary part of the refractive index to the highest single-scattering albedo (0.97) was 0.0015 at $\lambda = 0.55$ μm (Haywood et al. 2003). From ground-based measurements using the Aerosol Robotic Network (AERONET), the values of single-scattering albedo of MD higher than 0.95 at $\lambda = 0.67$, 0.87, and 1.02 μm were reported (Tanré et al. 2001; Dubovik et al. 2002; Kubilay et al. 2003) for the areas around the Sahara, the Middle East, and the Hawaiian Islands. Some possible reasons for stronger absorption properties in the early dust models compared with the recent results are the contamination of absorptive aerosols such as soot, inaccurate measurements, or lack of observed data. However, the present knowledge of optical properties over a wider spectral range is still insufficient, as reported by Sokolik et al. (2001).

Estimations of the global annual mean RF at TOA by MD for clear and cloudy skies using the climate model were close to zero (or heating), and were $+0.14$ W m^{-2} (Tegen et al. 1996), -0.075 W m^{-2} (Miller and Tegen 1998), $+0.02$ W m^{-2} (Miller and Tegen 1999), $+0.07$ W m^{-2} (Woodward 2001), and $+0.36$ W m^{-2} ($+0.26$ W m^{-2} for clear sky) (Takemura et al. 2002). In these models, relatively absorptive dust optical models were used, and thus the positive RFs were estimated over desert surfaces (Woodward 2001; Takemura et al. 2002). As mentioned previously, high single-scattering albedos of MD were primarily reported for Saharan dust. In those areas, local RF values in SW for clear sky estimated from airborne and satellite measurements over a desert surface were almost zero (Hsu et al. 2000) or negative (Haywood et al. 2003; Myhre et al. 2003; Li et al. 2004). Wang et al. (2004) showed that RF by MD could have both heating and cooling effects in the range of an assumed complex refractive index, even over the land in the simulation for spring 2001 in eastern Asia. Takemura et al. (2003) described the effects of anthropogenic aerosols and MD as comparable even in the Asian dust storm event in spring 2001.

There are many parameters which affect RF by MD. There is not only the imaginary refractive index and dust mineralogy (Claquin et al. 1998; Sokolik and Toon 1999), but also size distribution (Tegen and Lacis 1996; Myhre and Stordal 2001), surface albedo (Sokolik and Toon 1996; Liao and Seinfeld 1998), optical thickness (Liao and Seinfeld 1998), and vertical dust profile with cloud effects (Quijano et al. 2000; Takemura et al. 2002). However, to reduce the uncertainties of the effects of the optical and physical parameters of MD on RF, a more detailed sensitivity test of RF and global simulations with a chemical transport model are still necessary.

The Aeolian Dust Experiment on Climate Impact (ADEC) project was carried out from 2000 to 2004 mainly to estimate the amount of dust supplied from the surface to the atmosphere and radiative forcing by MD (Mikami et al. 2002). To investigate dust emission from the surface and its transportation process, a Model of Aerosol Species In the Global Atmosphere (MASINGAR) has been developed (Tanaka et al. 2003, 2005) to simulate the global distribution of MD. To estimate RF by MD simulated with MASINGAR for the atmospheric and MD profiles, we developed a Streamer-based Radiative Transfer Model for ADEC Sciences (SRTMAS) based on the model Streamer version 3.0 (Key 2001). The optimum calculation condition to calculate RF by MD from the output of MASINGAR is examined using SRTMAS, and sensitivities to some key parameters of RF caused by MD are investigated in this study.

2. SRTMAS

The radiative-transfer model SRTMAS developed in this study was partly recoded from a widely used radiative transfer model, Streamer version 3.0 (Key, 2001). The modified parts of the model are mainly databases of aerosols and spectral albedos and the radiative forcing calculation. Streamer uses the following radiation schemes: the discrete ordinate solver described in Stamnes et al. (1988), the two-stream method following Toon et al. (1989), the water-cloud optical properties from Hu and Stamnes (1993), the ice cloud optical properties from Ebert and Curry (1992), and the gas absorption data described in Tsay et al. (1989). Spectral resolution is 24 bands for SW and 109 bands for LW, which are generally high for estimating RF by aerosols from the chemical transportation model results. The advantages of using

such a spectrally detailed model are (1) to estimate the effect of spectrally detailed surface albedos on RF and (2) to avoid errors due to an insufficient spectral resolution of a radiative transfer model. We also have a choice for the number of streams, from a two-stream solver and discrete ordinate solver in the radiative transfer calculation, and will test this effect for the accuracy of RF.

2.1 Aerosol types

In SRTMAS, aerosol profiles simulated with MASINGAR, which are vertical profiles (30 layers) of MD with 10-bin size distribution from 0.1 to 10 μm in radius, sulfate (SA), sea salt (SS), black carbon (BC), and organic carbon (OC), are treated as an off-line input data. For the latter four aerosols, the typical size distribution from the OPAC database (Hess et al. 1998) is employed for each aerosol. Single-scattering parameters for aerosols such as single-scattering albedo (ω_0), asymmetry factor (g), and mass-extinction coefficient, are compiled in SRTMAS as apparently 14 types of aerosols (10 size bins for MD, and one for each of SA, SS, BC and OC). The calculations for the size distributions of the 14 types were made with the Mie theory using the refractive indices mentioned in the following section. In SRTMAS, the process of hygroscopic growth for aerosol particles (except MD) is employed using the same method as Chin et al. (2002).

2.2 Complex refractive index of MD

For the complex refractive index of MD, we used the mineral dust model in OPAC 3.1 (Hess et al. 1998) (OPAC-MD model) for all sensitivity tests of RF by MD, except for the sensitivity to refractive index (Section 4.1). In the MD refractive index test, two existing refractive index models and two original models were used. The former are the OPAC-MD model mentioned above and the Dust-Like model (Shettle and Fenn 1979). The latter original models were constructed by the following procedure, including *in situ* measurements with mineralogical methods. Three dust aerosol samples were collected with a cascade sampler around Qira (37°01′N, 80°44′E, 1363 m) in the Taklimakan Desert, China, April 12–14, 2002. The surface conditions of the sampling sites were gobi surface, sand dune, and oasis. Identified averaged mineral compositions are shown in Table 1.

Table 1. Averaged mineral compositions of three dust aerosol samples collected around Qira*1 from April 12 to 14, 2002.

Mineral	Volume fraction (%)
Illite*2	25.3
Calcite	15.3
Feldspar*2	10.7
Chlorite	10.7
Quartz*3	8.7
Dolomite	8.7
Halite	6.7
Gypsum	4.0
Kaolinaite*2	2.7
Magnesite	1.3
Other*4	0.7
Unknown	5.3

*1. Gobi site: 36°53′29″N, 80°47′01″E; sand dune site: 36°54′55″N, 80°46′48″E; oasis site: 37°00′56″N, 80°43′45″E.
*2. Spectral refractive indices in the shortwave region are compiled by Egan and Hilgemen (1979).
*3. Spectral refractive indices in the shortwave region are compiled in HITRAN96 (Rothman et al. 1998).
*4. Mineral contained Fe as major component.

The volume fraction of minerals for which the spectral refractive indices in the shortwave region have been compiled was 48% in the existing databases. From only this 48% of pure minerals, the composite spectral refractive index of MD at $\lambda \leq 3.0$ μm was obtained by weighted average of their refractive indices with the volume of each component. We refer to this refractive index model as ADEC-1 in this study. In this procedure, the refractive indices are referred from the databases by Egan and Hilgeman (1979) and HITRAN96 (Rothman et al. 1998) as shown in Table 1. Since the absorption of the ADEC-1 model is very weak compared with existing models, the model averaged from OPAC-MD and ADEC-1 was also made (ADEC-2 model). At $\lambda > 3.0$ μm in the ADEC-1 and ADEC-2 models, data in the OPAC-MD model were used. Spectral distribution comparisons of the complex refractive indices used in this study are shown in Fig. 1, together with those measured by AERONET for Saharan dust (Dubovik et al. 2002; Myhre et al. 2003).

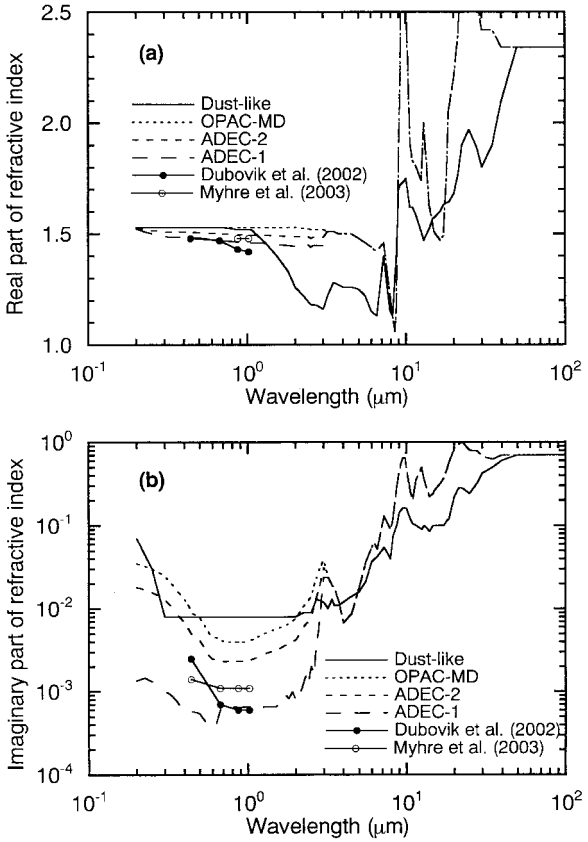

Fig. 1. Spectral distributions of complex refractive index of mineral dust models of Dust-like, OPAC-MD, ADEC-1, and ADEC-2 for (a) real part and (b) imaginary part. Observed values for Saharan dust at Cape Verde by AERONET (Dubovik et al. 2002; Myhre et al. 2003) are also shown for comparison.

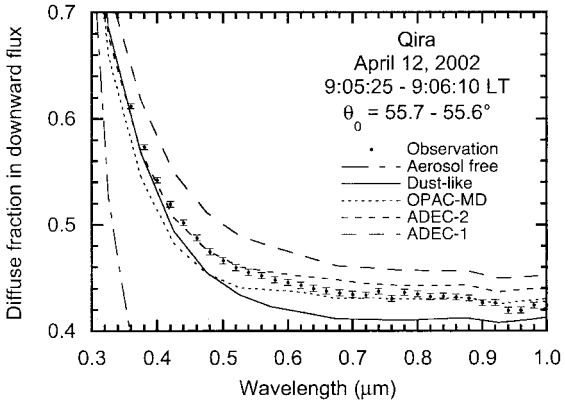

Fig. 2. Comparisons of measured spectral distributions of diffuse fraction in downward flux with the theoretically calculated ones on April 12, 2002, at the oasis site in Qira. Aerosol optical thickness was 0.4 at $\lambda = 0.5$ μm. Observed values are shown by dots with standard deviation shown by error bars. Standard deviation was calculated from five measured spectra of diffuse fraction.

Since the ADEC-1 and ADEC-2 models are not physically rigorous (only a half mineral composition is considered in the ADEC-1 model, and the ADEC-2 model is a simple average between the ADEC-1 and OPAC-MD models), we checked the validity of these models together with the other two models from the field measurements. Spectral diffuse fractions in downward flux were observed with a spectrometer ("FieldSpec Pro JR" of ASD Inc.) on April 12, 2002 during the aerosol sampling period at the oasis site in Qira (Table 1). The measured spectral diffuse fractions in downward flux were compared with the theoretically calculated ones using four refractive index models. In these calculations, we employed the size distribution of the Desert model in OPAC 3.1 (Hess et al. 1998) because in situ measured size distribution on the ground around Qira was extremely coarse. Figure 2 shows example of this comparison, where τ_{MD} was 0.4 at $\lambda = 0.5$ μm from the measurement by the sky radiometer. Measured diffuse fractions agree with the calculated one using the ADEC-2 model at $\lambda \leq 0.5$ μm, however, it was shifting to the calculated one using the OPAC-MD model at longer wavelengths. Some of measured diffuse fractions in other time periods of the same day agreed with the OPAC-MD model rather than the ADEC-2 model. Therefore, it is considered that the refractive index of MD falls in the range between the ADEC-2 and OPAC-MD models. However, the spectral distribution of diffuse fractions could be changed not only by refractive index but also by aerosol size distribution. Thus, it will be difficult to accurately determine the complex refractive index of MD by this method. However, these four models cover the possible range of the refractive index by considering the measured refractive indices for Saharan MD shown in Fig. 1. For the complex refractive indices of the other aerosols, the data compiled by Shettle and Fenn (1979) are employed for SA, SS, and BC, and the water-

Table 2. Location information and basic optical properties of aerosols at four locations used in the radiative transfer calculation.

Location	Japan	Tarim	Sahara	Siberia
Latitude	34°30′25″N	40°06′11″N	25°10′48″N	64°11′04″N
Longitude	136°52′30″E	84°22′30″E	9°22′30″E	129°22′30″E
Surface type	Sea	Desert	Desert	Snow
Albedo model*1	Open sea	Sand dune	Pixel-W	Fresh snow
Broadband albedo	0.024	0.273	0.357	0.703
Date in 2002	April 28	April 4	April 19	April 18
τ_{MD}*2	0.513	0.809	0.878	0.154
ω_0*3 of MD	0.935	0.928	0.917	0.934
g*4 of MD	0.694	0.699	0.707	0.694
τ*2				
Sulfate (SA)	0.075	0.053	0.052	0.075
Sea salt (SS)	0.020	0.013	0.013	0.021
Black carbon (BC)	0.004	0.004	0.004	0.004
Organic carbon (OC)	0.004	0.003	0.003	0.004

*1. Detailed spectral distribution will be shown in Fig. 10.
*2. Optical thickness at $\lambda = 0.55$ μm.
*3. Single-scattering albedo at $\lambda = 0.55$ μm. These values are calculated from ω_0 in each dust layer by weighted-average with τ_{MD} in each layer.
*4. Asymmetry factor of MD. Optical properties of MD are calculated by the OPAC-MD model.

soluble model by Shettle and Fenn (1979) is used for OC.

2.3 *Aerosol and atmospheric information from MASINGAR*

Aerosol and atmospheric profiles from MASINGAR are daily means, and therefore, in SRTMAS the diurnally averaged RFs by aerosols are calculated by the following method: For SW, instantaneous RFs at hourly solar zenith angles (θ_0) including local solar noon are calculated and averaged to get a diurnally averaged RF. For LW, only one calculation is made for daily mean profiles of aerosols and atmosphere and daily mean surface temperature. For the RF sensitivity tests to different MD profiles and locations, we used four types of outputs from MASINGAR: over the sea off Japan, the desert in Tarim Basin and the Sahara Desert, and snow in Siberia, all for the spring season as shown in Table 2 and Fig. 3. For Tarim and the Sahara, the MD is just under the outbreak and thus a large optical thickness (τ_{MD}) at $\lambda =$ 0.55 μm is simulated (Fig. 3a). For Japan, the dense MD ($\tau_{MD} \sim 0.5$) is transported to this region and distributed at the peak height of 6 km (Fig. 3a), and the amount of MD in Siberia is relatively small. Size distribution of MD is large in the desert areas, with that in the Sahara being somewhat larger than that in Tarim, while Japan and Siberia have small distributions (Fig. 3b). Aerosol profiles other than MD are assumed to be the same in the four locations to maintain the same condition for the sensitivity tests of RF by MD (Fig. 3c). However, wet weight profiles differ due to the hygroscopic growth of aerosol particles.

2.4 *Spectral albedo*

In the original Streamer 3.0, 12 spectral albedo datasets were prepared. However, they were insufficient for desert (only "Dry sand") and snow/ice cover ("Meltponds on sea ice," "Melting snow," "Fresh snow," and "Bare ice"). Thus, we added nine spectral albedos for the desert surface in SRTMAS, of which seven spectra were measured in situ in Chinese deserts (Aoki et al. 2002, 2005), and two were satellite-derived spectra from different locations in the Sahara Desert (Acarreta and Stammes 2003). Since the spectral range of albedos measured with a spectrometer in Chinese deserts is from 0.35 to 2.5 μm, the spectral albedos at $\lambda < 0.35$ μm are extrapolated and the values at $\lambda = 2.5$ μm are used at $\lambda > 2.5$ μm. For snow surfaces, 18 theo-

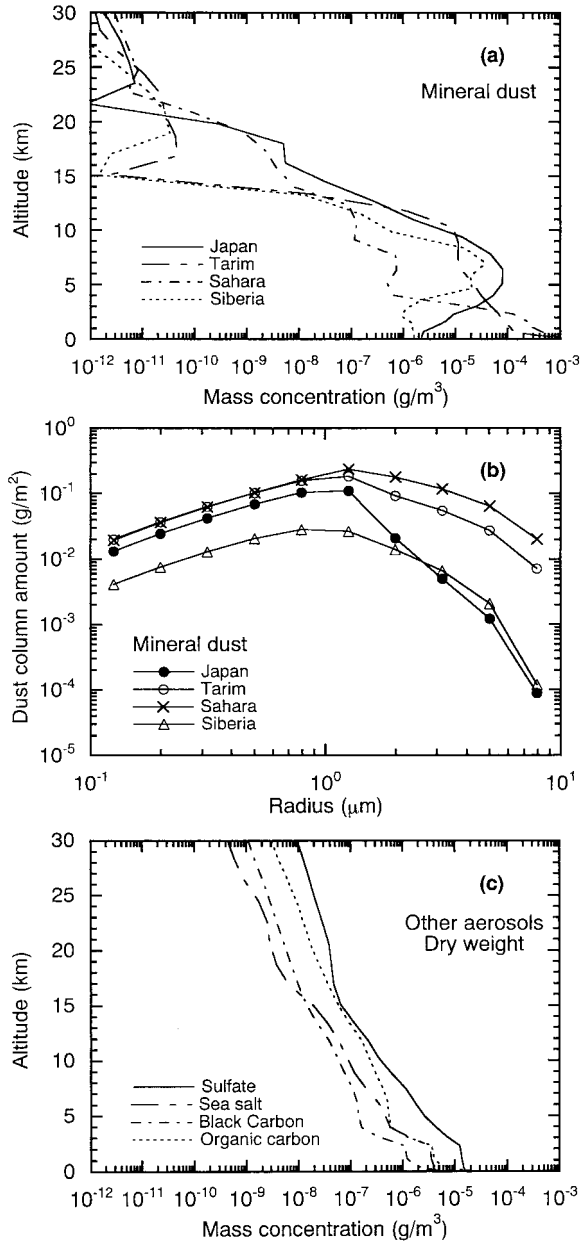

Fig. 3. (a) Vertical profiles of MD mass concentration calculated with MASINGAR in four locations: Japan, Tarim, Sahara, and Siberia, at which surface conditions are shown in Table 1. (b) Column amounts for those four profiles of MD. (c) Vertical profiles of dry mass concentrations of sulfate, sea salt, black carbon, and organic carbon.

retically calculated spectral albedos were added, where the spectral albedo varies depending on snow grain size and concentration of snow impurities (Aoki et al. 1999, 2000). Spectral albedo data used for standard sensitivity tests of RF by MD are "Open sea" for Japan, "Sand dune in the southern Taklimakan Desert" (in situ measured data) for Tarim, "Pixel-W in Sahara Desert" (satellite-derived data) for the Sahara, and "Fresh snow" for Siberia. "Open sea" and "Fresh snow" are datasets from the original Streamer model. The broadband albedos calculated in SRTMAS for these four surfaces are shown in Table 2. For the sensitivity test of RF by MD to the effect of spectral surface albedo, which will be described in Section 4.3, the other data of spectral albedos are also used. The sky conditions are assumed to be clear in all RF calculations except for the effects of cloud cover, which will be described in Section 4.4.

3. Influence of calculation method on RF accuracy

3.1 Number of streams

Radiative forcing calculation for the global dataset is a time-consuming task, so it is necessary to examine the trade off between calculation time and expected accuracy for RF. We thus used the flexibility of the number of streams for the calculation of radiative transfer in the Streamer and tested the effect of the number of streams on the accuracy of RF by MD. Figure 4 shows the results for four locations using the OPAC-MD model, which also include the other four types of aerosols. In the SW region, the values of RF produced by the two-stream solver differ from the values produced by solvers with four or more streams, and RFs produced by the solvers with four or more streams agree well with each other. In the LW region, good agreement is obtained from all solvers, including the two-stream solver. Thus, we can expect an accurate result for RF with a four-stream solver for both SW and LW. However, the two-stream solver is also acceptable only for LW. In the present study, we used the four-stream solver for both SW and LW.

3.2 Influence of all aerosols other than MD

When several types of aerosols are contained in the atmosphere, RF by MD is also likely to

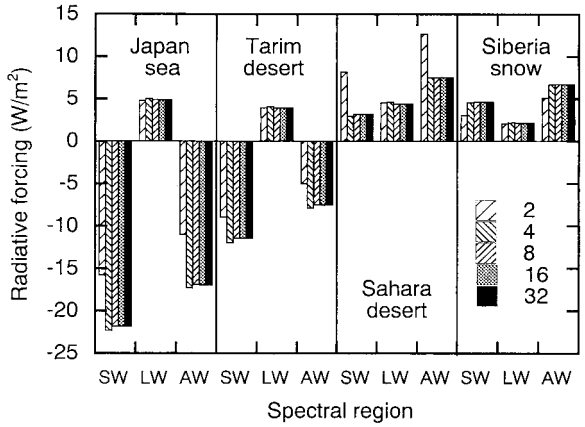

Fig. 4. Diurnally averaged RF by MD at TOA under clear sky conditions calculated using 2 to 32 streams with SRTMAS at four locations. Calculations are made for the shortwave (SW), the longwave (LW), and the shortwave+ longwave (AW) spectral regions under clear-sky conditions.

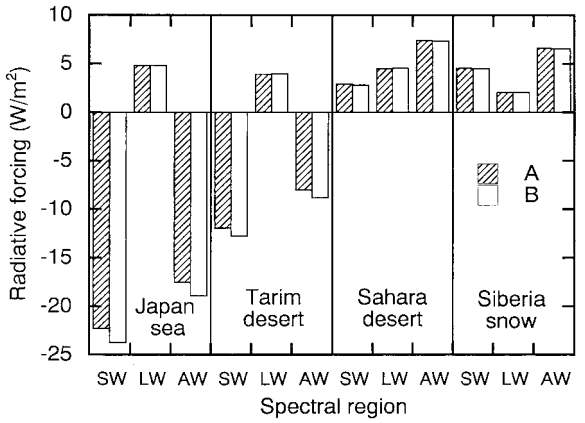

Fig. 5. Same as Fig. 4, but calculated using the following two different methods. (A) Difference in net radiation between a case containing all aerosols and a case containing all aerosols except MD. (B) Difference in net radiation between MD-only case and an aerosol-free case.

be affected by other aerosols. There are two methods for calculating RF by MD: (A) the difference in net radiation between a case containing all aerosols and a case containing all aerosols except MD; and (B) the difference in net radiation between MD-only case and an aerosol-free case. Figure 5 illustrates the results of RF by MD at TOA for four locations. Maximum error, that is the difference between methods (A) and (B), was less than 10% in any spectral region of SW, LW, and SW+LW. Essentially, the RF should be calculated by method (A). In the present study, we used this method.

The following three calculation methods are considered to calculate the total RF produced by all aerosols: (A′) the sum of RFs for all aerosols in which each RF is calculated from the difference in net radiation between a case containing all aerosols and a case containing all aerosols except one; (B′) the sum of RFs for all aerosols in which each RF is calculated from the difference in net radiation between a case containing one aerosol and an aerosol-free case; and (C′) the difference in net radiation between a case containing all aerosols and an aerosol-free case. The results of the RFs at TOA for Japan and Siberia are shown in Fig. 6, where the contributions to the total RF from each aerosol are also shown. The difference between methods (A′) and (B′) is also seen in aerosols other than MD. The total radiative effect from all aerosols should be calculated by method (C′). This result does not completely agree with those by methods (A′) and (B′). In particular, the difference for SW radiation over snow in Siberia is larger than that over the sea. Over the snow surface, the difference is enhanced by multiple reflection of SW radiation between the atmosphere and the high albedo surface, where the presupposed aerosol conditions in the atmosphere differ among the three methods.

4. Effects of MD properties, atmosphere, and surface condition on RF

4.1 Complex refractive index and solar zenith angle

The most important effect in optical properties of MD on RF is the complex reflective index, particularly the imaginary part in the SW region. As described in Section 1, the most current observational results demonstrated that light absorption by Saharan dust is very weak compared with those previously considered. However, mixing with more absorptive aerosols could increase the absorption by MD. We examined the effects of refractive indices of MD

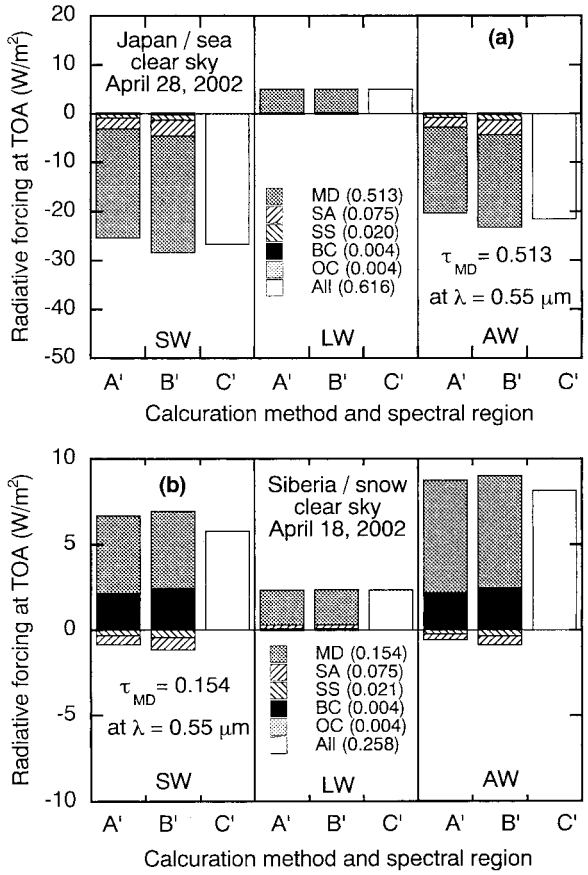

Fig. 6. Diurnally averaged RF by MD at TOA under clear sky conditions for (a) Japan and (b) Siberia calculated using the following three methods. (A′) The sum of RFs for all aerosols in which each RF is calculated from the difference in net radiation between a case containing all aerosols and a case containing all aerosols except the target aerosol. (B′) The sum of RFs for all aerosols in which each RF is calculated from the difference in net radiation between a case containing one aerosol and an aerosol-free case. (C′) The difference in net radiation between a case containing all aerosols and an aerosol-free case.

on RF using four refractive indices, the Dust-Like model, the OPAC-MD model, the ADEC-1 model, and the ADEC-2 model. Considering our analysis process to determine the refractive index mentioned in Section 2, these four models should cover the possible range of absorption by MD. Figure 7 presents the instantaneous RF by MD in SW at TOA as a function of θ_0 for these four refractive indices at four locations. Since the sensitivity of instantaneous RF to the refractive index of MD varies with the conditions of albedo and θ_0, the instantaneous RFs by MD are calculated for different surface conditions (albedos) and are all in range of θ_0. The θ_0 dependence of the instantaneous RF is not linear. This is basically explained by the same effect as the θ_0 dependence of surface albedo on scattering media. At any location, RFs are in the order of absorption of MD models (Dust-Like, OPAC-MD, ADEC-2, and ADEC-1). In the figure, the sensitivities of RF depend on many factors, such as MD model (difference in refractive index), albedo, τ_{MD}, and θ_0. To examine the cause of variability of RF by the differences in MD models, the differences in RFs between the Dust-Like model and ADEC-1 model at $\theta_0 = 60°$ are divided by τ_{MD}, because the RF by MD varies linearly with τ_{MD} (Liao and Seinfeld 1998). This value is interpreted to be the sensitivity of instantaneous RF per unit τ_{MD} to the difference in MD models (refractive index). The results were 33.4 W m^{-2} for Japan (albedo 0.024), 44.0 W m^{-2} for Tarim (albedo 0.273), 55.6 W m^{-2} for Sahara (albedo 0.357), and 123.9 W m^{-2} for Siberia (albedo 0.703). These values of sensitivity of instantaneous RF increase with albedo except for large solar zenith angles ($\theta_0 > 80°$). Namely, the sensitivity of RF to the refractive index strongly depends on albedo. The effect of the difference in the MD model on RF is remarkable over high albedo surfaces and the effect is relatively small over the sea. This is because the multiple reflection between the atmosphere (dust) and the surface enhances the light absorption by dust particles over a high-albedo surface.

Over desert surfaces in Fig. 7, RF could take both positive and negative values in the range of MD models over a wide range of θ_0, especially for the Sahara. From this point of view, the refractive index of MD is important in determining the sign of RF over the desert surface. The difference in RFs over desert surfaces between Tarim and Sahara is due to the difference in albedo, size distribution (thus, ω_0 and g), and τ_{MD}. The effects of albedo and size distribution will be discussed in the next section.

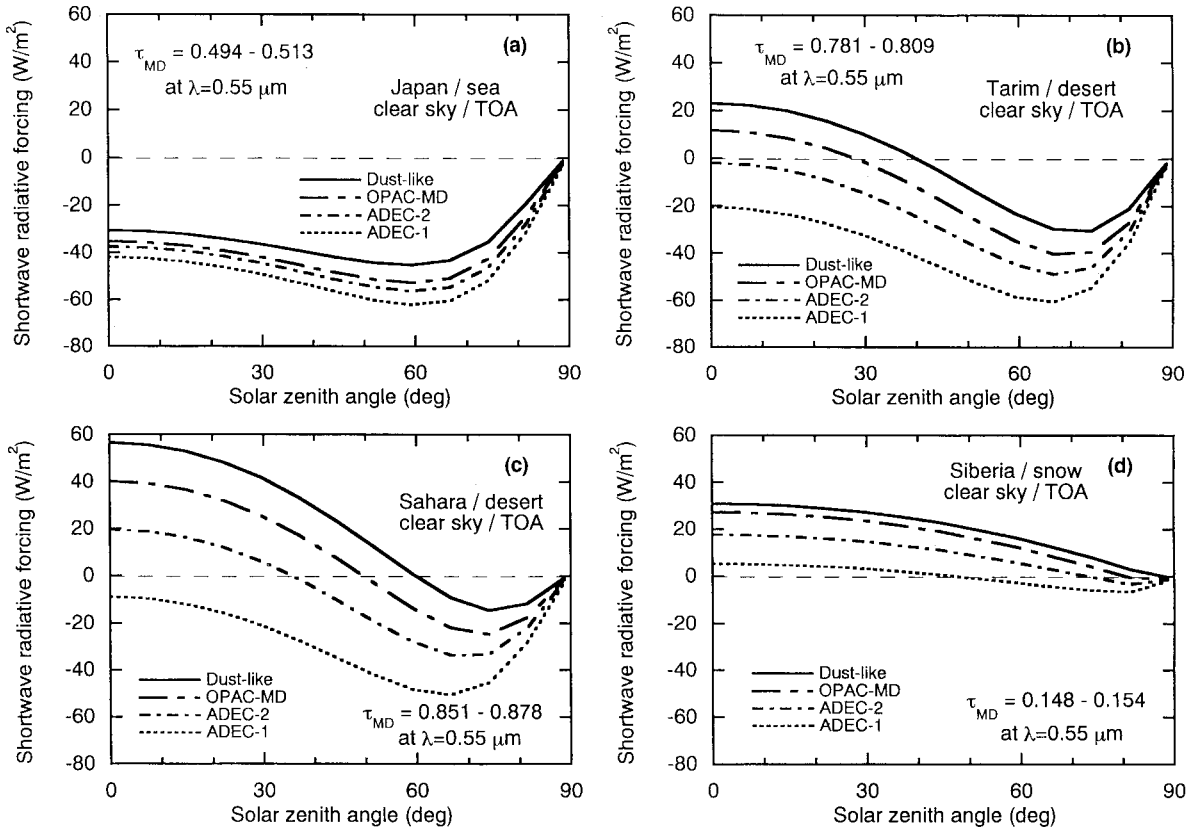

Fig. 7. Instantaneous RF by MD in SW at TOA under clear sky conditions as a function of solar zenith angle calculated using four refractive indices (Dust-like, OPAC-MD, ADEC-1, and ADEC-2) shown in Fig. 1 for (a) Japan, (b) Tarim, (c) Sahara, and (d) Siberia.

4.2 Broadband surface albedo and size distribution over the desert surface

Liao and Seinfeld (1998) showed that the surface albedo at which the sign of RF by MD in SW at TOA changes from negative to positive is 0.3. The desert surface albedo corresponds approximately to this value. As we have seen in the previous section, instantaneous RF by MD in SW at TOA varies strongly with θ_0 over the desert surface, and thus, RF could vary depending on season or latitude if the MD and atmospheric conditions are the same. However, the desert surface albedo also differs depending on surface conditions (Aoki et al. 2002, 2005). We examined the variability of RF with the desert surface albedo and the season, that is, the difference in diurnal variation of θ_0 under the fixed conditions of MD and atmosphere. Figure 8 shows the diurnally averaged RF by MD in SW at TOA as a function of broadband albedo for three specific days: one day in spring (original date), the winter solstice, and the summer solstice. In these calculations, the atmospheric and aerosol conditions are fixed as shown in Table 2, and only the conditions of surface albedo and θ_0 are assumed to be varied. The broadband albedos employed were measured in situ in China and derived by satellite over the Sahara Desert. This is a possible range in broadband albedo of desert surface. Figure 8 demonstrates that the RF can take both positive and negative values in this range of albedo. The surface albedo at which the sign of RF by MD in SW at TOA changes from negative to positive exceeds 0.36 (0.32) in Tarim (the Sahara). The figure shows the RF changes with the conditions of dust, location, and season. In Fig. 8, the value of RF varies linearly with albedo in any season for both Tarim and the Sahara. The difference in slope

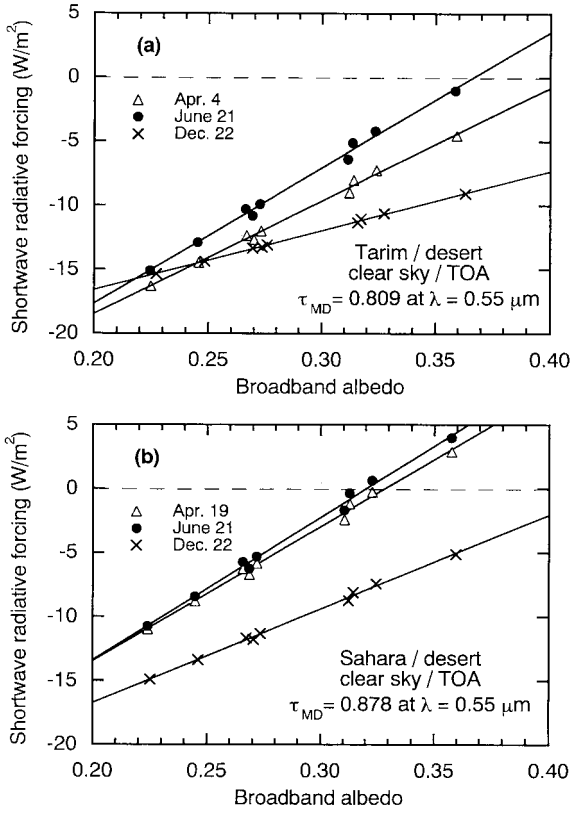

Fig. 8. Diurnally averaged RF by MD in SW at TOA under clear sky conditions for (a) Tarim and (b) Sahara as a function of broadband albedo for three specific days; the original date in spring (April 4 in (a) and April 19 in (b)), the winter solstice (December 22) and summer solstice (June 21). For the winter and summer solstices, only the condition of diurnal variation of θ_0 differs from that in spring; the atmospheric and dust aerosol conditions are the same as those in spring.

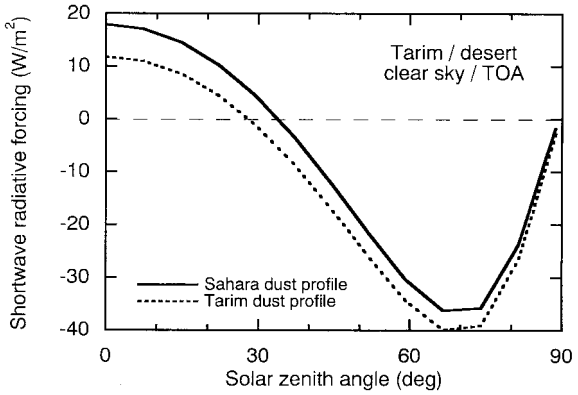

Fig. 9. Solar zenith angle dependence of instantaneous RF by MD in SW at TOA in Tarim under clear sky conditions. One is the original dust condition in Tarim and the other is the result in which only the dust condition (profile and size distribution) of the Sahara is assumed in the case of Tarim.

is mainly due to the difference in diurnal variations of θ_0 which changes depending on location and season. The θ_0 dependence of instantaneous RF is not linear, as shown in Fig. 7, but instantaneous RF increases with θ_0 at $\theta_0 > 70°$. Therefore, the diurnally averaged RF is large in summer.

In Fig. 8, the surface albedo at which the sign of RF changes is lower in the Sahara than in Tarim. This is because in the Sahara, (1) the values of θ_0 are smaller, (2) the size distribution is larger and thus ω_0 is lower and g is larger, and (3) the value of τ_{MD} is somewhat larger. If only the dust condition (profile and size distribution) of the Sahara is assumed in the case of Tarim, and other conditions (albedo, atmosphere except dust, and θ_0 variation) are kept the same as those of Tarim, the instantaneous RF in SW at TOA for the Sahara dust profile is higher than that in the original case of Tarim at any value of θ_0 as shown in Fig. 9. This difference in RF is primarily due to the difference in size distribution of MD. In the case of large dust particles of the Sahara, the values of ω_0 (g) are lower (larger) than those in Tarim, as shown in Table 2. Both of these effects lead to a larger RF in the Sahara than in Tarim. This variability of RF due to the variation in size distribution is approximately half of the difference in RF between the OPAC-MD and ADEC-2 models of refractive index at any θ_0 shown in Fig. 7b. Myhre and Stordal (2001) showed that the effect due to variation of size distribution of MD on RF is comparable to that by variability of the refractive index.

4.3 Spectral surface albedo

The effect of broadband surface albedo on RF by MD in SW at TOA over the desert surface is shown in the previous section. However, optical properties of MD vary depending on the wave-

length. For long-distance transported MD with a small effective radius (less than 0.6 μm), the value of τ_{MD} in the visible region is generally larger than that in the near infrared region. The effect of spectral distribution of surface albedo on MD is therefore examined for various surfaces. Figure 10 plots the spectral surface albedos of snow and ice, deserts, and vegetation in the SW region. Spectral snow albedos in Fig. 10a are calculated by a multiple-scattering radiative transfer model for the atmosphere-snow system (Aoki et al. 1999, 2000) as functions of snow grain radius (r) and mass concentration of snow impurities (c). Bare ice albedo is compiled in Streamer 3.0. For the desert surface albedos shown in Fig. 10a, the first seven albedos were measured in situ in China (details are described in Aoki et al. 2005), and the next two albedos were derived by Acarreta and Stammes (2003) from satellite measurements in the Sahara Desert. These desert albedos are the same as those used in Fig. 8. "Dry sand" is compiled in Streamer 3.0. For vegetation surfaces, five spectral vegetation albedos are used from the dataset in Streamer 3.0.

When a spectral surface albedo is assumed, the broadband albedo is calculated by SRTMAS under given atmospheric and dust conditions. Figure 11 illustrates the diurnally averaged RFs by MD in SW for the TOA, surface, and atmosphere as a function of broadband albedo, when different spectral surface albedos are assumed under the atmospheric and dust conditions of Siberia. For this case, the effective particle radius of MD is 0.56 μm, which is calculated from the column amount of MD (Fig. 3b). In Fig. 11, open symbols indicate snow and ice surfaces, and solid symbols are desert and vegetation surfaces. In general, broadband surface albedos of snow and ice are high and those of desert and vegetation are low. For an albedo range from 0.30 to 0.44, both symbols coexist, where RFs for snow and ice surfaces are larger than those for desert and vegetation surfaces in all cases for the TOA, surface, and atmosphere. This is because spectral albedos of snow and ice surfaces are generally higher in the visible region than those in the near infrared region, while for desert and vegetation surfaces, this spectral situation is the reverse. However, the extinction coefficient of MD in the visible region is larger than that in the near infrared region

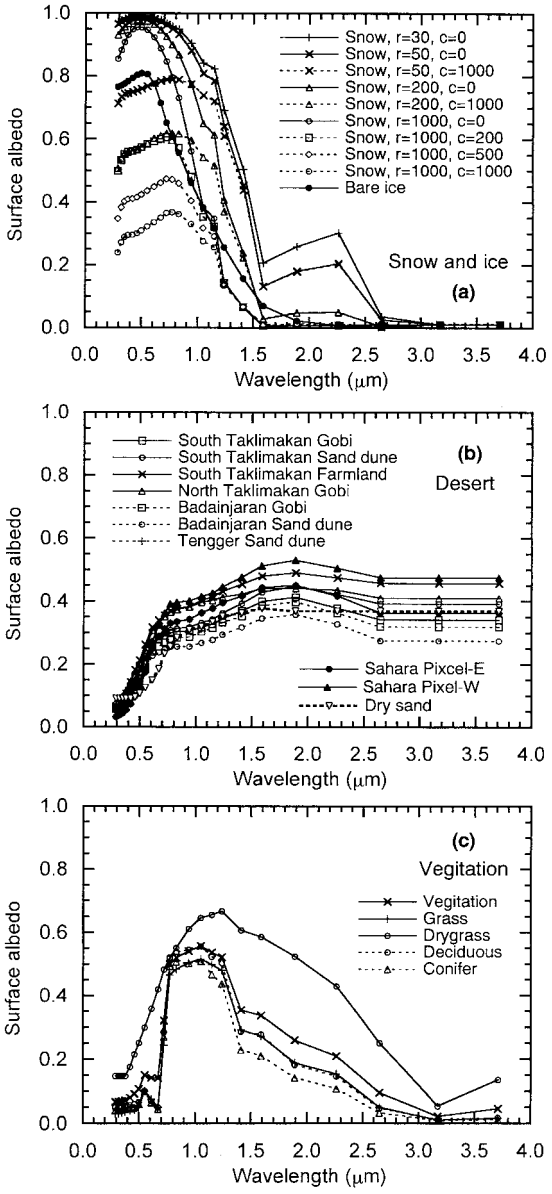

Fig. 10. Spectral surface albedos of (a) snow and ice, (b) deserts, and (c) vegetation in the shortwave region. Spectral albedos of snow surface were theoretically calculated as functions of snow grain radius (r) and mass concentration of snow impurities (c). Desert surface albedos were measured in situ in China and derived by satellite in the Sahara except for "Dry sand," which is compiled in Streamer 3.0. Vegetation albedos were employed from the dataset compiled in Streamer 3.0.

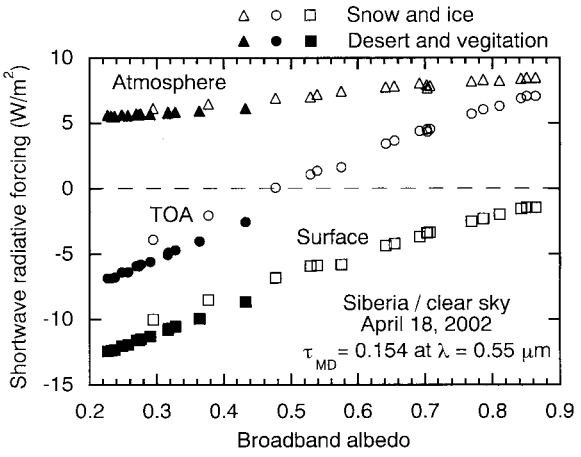

Fig. 11. Diurnally averaged RF by MD in SW for the TOA, surface, and atmosphere as a function of broadband albedo under clear sky conditions. The dust and atmospheric conditions are the same as in Siberia, but only the spectral surface albedo is changed using those shown in Fig. 10. Open symbols indicate snow and ice surfaces, and solid symbols, desert and vegetation surfaces.

for this MD condition in Siberia. Therefore, one should notice that RF by MD could change depending on the difference in surface type even if the broadband albedo is the same. This tendency would be remarkable for smaller aerosols because the extinction coefficient is larger at shorter wavelengths.

4.4 Cloud cover

For the real atmosphere, the effect of cloud cover is an important factor for estimating the RF by MD. It is reported that RF by MD over the sea surface strongly depends on the relationship between cloud height and the vertical profile of MD (Quijano et al. 2000; Takemura et al. 2002). We also examined the effect of cloud cover on RF for the four locations we used. Figure 12 shows the RFs by MD in SW+LW at TOA as a function of a cloud water path for three cases of cloud covers; two cases of water clouds in low levels and a case of ice cloud around the height of 10 km. In the case of the lowest cloud layer (Fig. 12a), the MD layers in Japan and Siberia (Fig. 3a) are higher than

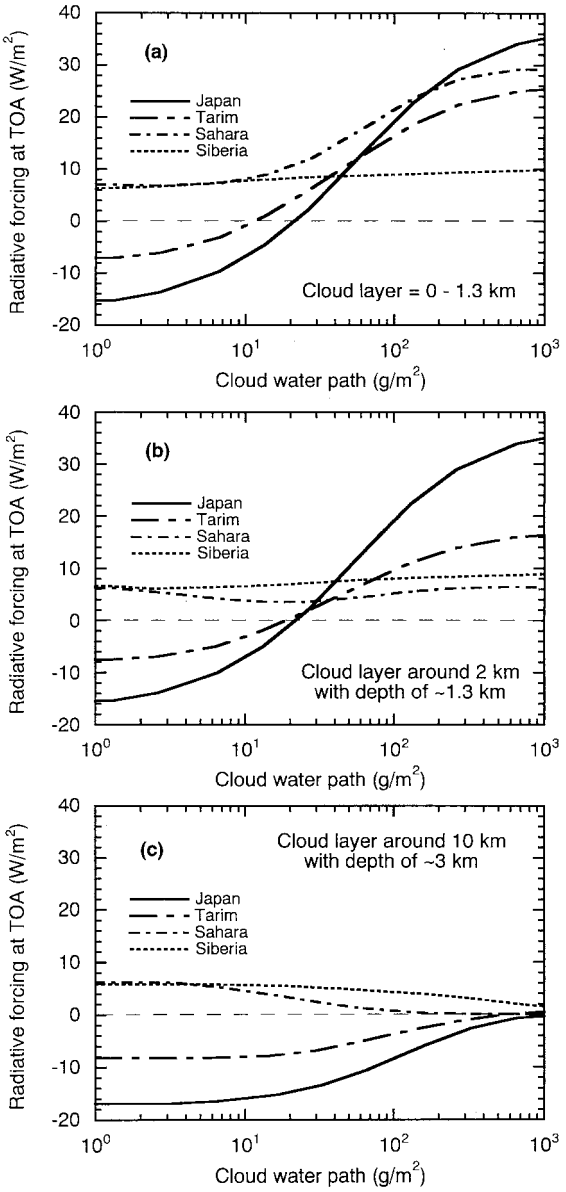

Fig. 12. Diurnally averaged RF by MD in all wavelength regions at TOA as a function of a cloud water path for four locations. Cloud types are (a) water cloud in the layer of 0 to 1.3 km, (b) water cloud at 2 km with a thickness of 1.3 km, and (c) ice cloud at 10 km with a thickness of 3 km. The exact height and thickness of cloud cover differ somewhat in each atmospheric profile at the four locations. Effective cloud particle radius is assumed to be 10 μm for water clouds and 30 μm for spherical ice cloud.

the cloud layer (0 to 1.3 km). Although MD peaks in Tarim and the Sahara are at the same level as the cloud layer, a large amount of MD is still distributed above the cloud layer. Cloud cover thus acts to increase RF by MD with a cloud water path. For the second case (Fig. 12b), where cloud height increases to about 2 km, the cloud effects on RF in Tarim and the Sahara decrease. In both Figs. 12a and 12b, the cloud effect in Siberia is very weak because the cloud albedo and underlying snow albedo are very close to each other. The third case of high clouds (Fig. 12c) differs from the other two. The absolute value of RF in any location decreases and approaches zero with an increase of cloud water path. We also conclude that the vertical relation of cloud cover to the MD layer is important over desert and sea surfaces. However, the effect of cloud cover on RF is generally small over a snow surface.

5. Summary

The radiative transfer model SRTMAS was developed based on Streamer version 3.0 in order to estimate the direct radiative forcing by MD using the atmospheric and MD profiles calculated with the chemical transport model MASINGAR. The characteristics of SRTMAS are (1) it is a spectrally detailed model, (2) it employs five types of aerosols including 10-bin-sized MD, and (3) it provides in situ measured spectral albedos of Chinese deserts and abundant theoretically calculated spectral albedos for snow. Experiments were conducted to determine the sensitivity of RF by MD to the optical properties of MD, surface albedo, solar zenith angle, and cloud cover for four dust profiles simulated with MASINGAR at four locations: the sea off Japan, the desert in Tarim Basin, the Sahara Desert, and snow in Siberia.

The optimum calculation conditions to estimate RF at TOA are tested to determine the effect of the number of streams used in SRTMAS on the accuracy of RF, and the influence of all aerosols (other than MD) on RF by MD, or all aerosols. A four-stream solver has acceptable accuracy for RF by MD at TOA in the SW region, and a two-stream solver has acceptable accuracy in the LW region. When several types of aerosols are contained in the atmosphere, the test results showed that the RF by MD should not be calculated from the difference in net radiation between MD-only case and an aerosol-free case, but the difference in net radiation between a case containing all aerosols and a case containing all aerosols except MD. Regarding the influence of each aerosol to RF produced by all five types of aerosols, it should be noted that RFs calculated by the following two methods do not completely agree: (1) the sum of all 5 RFs for each aerosol calculated from the difference in net radiation between a case containing all aerosols and a case containing all aerosols except the target aerosol; and (2) the difference in net radiation between a case containing all aerosols and an aerosol-free case. Although both RFs are conceptually the RF by all aerosols, the radiative interactions among aerosols are not considered in the former methods. The difference between the two methods was larger over snow surfaces than over the sea.

It was found that the sensitivity of instantaneous RF by MD in SW at TOA to refractive index strongly depends on albedo. Namely, the effect of the differences in MD models on instantaneous RF is significant over high albedo surfaces and is relatively small over the sea. This is because the multiple reflection between the atmosphere (dust) and surface enhances light absorption by dust particles over high albedo surfaces. Over desert surfaces, the instantaneous RF by MD in SW at TOA could take both positive and negative values in the possible range of refractive indices of MD, which are two widely used models (Dust-like and OPAC-MD) and the original two models (ADEC-1 and ADEC-2) determined from mineralogy analysis for dust and spectral radiation observation in China. Over desert surfaces, the diurnally averaged RF in SW at TOA could also take both positive and negative values in the possible ranges of desert albedo, which are in situ measured albedos in China and satellite-derived albedos in the Sahara. MD size distribution is the next most important factor for the RF.

The effect of spectral distribution of surface albedo on RFs by MD in SW for the TOA, surface, and atmosphere is examined for various surfaces. For small dust particles with an effective radius of less than 0.6 μm, RFs by MD could change depending on the difference in surface type even if the broadband albedo is the same. This is due to the contrast of the spectral

distribution between the albedo and the extinction coefficient of MD. RF at TOA in all spectral regions is very sensitive to the vertical positional relationship between cloud cover and dust layer over desert and sea surfaces. However, the effect of cloud cover is generally small over snow surfaces, because cloud albedo and underlying snow albedo are very close to each other.

Acknowledgments

This work was conducted as part of the Aeolian Dust Experiment on Climate Impact (ADEC) project from 2000 to 2004 supported by the Ministry of Education, Culture, Sports, Science and Technology of Japan. We would like to express our appreciations to Ms. Reiko Watanabe and Mr. Richard Cripe who assisted in English-language manuscript revision. We are also grateful to anonymous reviewers who provided valuable comments.

References

Acarreta, J.R. and P. Stammes, 2003: Verification of Sciamachy's reflectance over the Sahara. *Proc. Envisat Validation Workshop*, 9–13 December 2002 ESRIN, Frascati, Italy, available from http://envisat.esa.int/pub/ESA_DOC/envisat_val_1202/proceedings/ACV/SCIAMACHY/02_acarreta.pdf.

Aoki, Te., Ta. Aoki, M. Fukabori, and A. Uchiyama, 1999: Numerical simulation of the atmospheric effects on snow albedo with a multiple scattering radiative transfer model for the atmosphere-snow system. *J. Meteorol. Soc. Japan*, **77**, 595–614.

———, ———, ———, A. Hachikubo, Y. Tachibana, and F. Nishio, 2000: Effects of snow physical parameters on spectral albedo and bidirectional reflectance of snow surface. *J. Geophys. Res.*, **105**, 10219–10236.

———, M. Mikami, and W. Liu, 2002: Spectral albedos of desert surfaces and size distributions of soil particles measured around Qira and Aksu in Taklimakan Desert. *J. Arid Land Studies*, **11**, 259–266.

———, ———, A. Yamazaki, S. Yabuki, Y. Yamada, M. Ishizuka, F. Zeng, W. Gao, J. Sun, L. Liu, and M. Zhou, 2005: Spectral albedo of desert surfaces in central and western China. *J. Meteorol. Soc. Japan*, **83A**, 279–290.

Chin, M., P. Ginoux, S. Kinne, O. Torres, B. Holben, B.N. Duncan, R.V. Martin, J.A. Logan, A. Higurashi, and T. Nakajima, 2002: Tropospheric aerosol optical thickness from the GOCART model and comparisons with satellite and sun photometer measurements. *J. Atmos. Sci.*, **59**, 461–483.

Chou, C.C.-K., T.-K. Chen, S.-H. Huang, and S.C. Liu, 2003: Radiative absorption capability of Asian dust with black carbon contamination. *Geophys. Res. Lett.*, **30**, 1616, doi:10.1029/2003GL017076.

Claquin, T., M. Schulz, Y. Balkanski, and O. Boucher, 1998: Uncertainties in assessing radiative forcing by mineral dust. *Tellus*, **50B**, 491–505.

d'Almeida, G.A., 1987: On the variability of desert aerosol radiative characteristics. *J. Geophys. Res.*, **92**, 3017–3026.

Dubovik, O., B. Holben, T.F. Eck, A. Smirnov, Y.J. Kaufman, M.D. King, D. Tanré, and I. Slutsker, 2002: Variability of absorption and optical properties of key aerosol types observed in worldwide locations. *J. Atmos. Sci.*, **59**, 590–608.

Ebert, E.E. and J.A. Curry, 1992: A parameterization of ice cloud optical properties for climate models. *J. Geophys. Res.*, **97**, 3831–3836.

Egan, W.G. and T.W. Hilgeman, 1979: *Optical Properties of Inhomogeneous Materials: Applications to Geology, Astronomy, Chemistry and Engineering*, Academic Press, San Diego, Calf., 235pp.

Hansen, J., M. Sato, and R. Ruedy, 1997: Radiative forcing and climate response. *J. Geophys. Res.*, **102**, 6831–6864.

Haywood, J.M., P.N. Francis, M.D. Glew, and J.P. Taylor, 2001: Optical properties and direct radiative effect of Saharan dust: A case study of two Saharan dust outbreaks using aircraft data. *J. Geophys. Res.*, **106**, 18417–18430, 10.1029/2000JD900319.

———, ———, S. Osborne, M. Glew, N. Loeb, E. Highwood, D. Tanré, G. Myhre, P. Formenti, and E. Hirst, 2003: Radiative properties and direct radiative effect of Saharan dust measured by the C-130 aircraft during SHADE: 1. Solar spectrum. *J. Geophys. Res.*, **108**, 8577, doi:10.1029/2002JD002687.

Hess, M., P. Koepke, and I. Schult 1998: Optical properties of aerosols and clouds: The software package OPAC. *Bull. Am. Met. Soc.*, **79**, 831–844.

Hsu, N.C., J.R. Herman, and C. Weaver, 2000: Determination of radiative forcing of Saharan dust using combined TOMS and ERBE data. *J. Geophys. Res.*, **105**, 20649–20661.

Hu, Y.X. and K. Stamnes, 1993: An accurate parameterization of the radiative properties of water

clouds suitable for use in climate models. *J. Climate*, **6**, 728–742.

IPCC, 2001: *Climate Change 2001: The Scientific Basis. Contribution of Working Group I to the Third Assessment Report of the Intergovernmental Panel on Climate Change* [Houghton, J.T., Y. Ding, D.J. Griggs, M. Noguer, P.J. van der Linden, X. Dai, K. Maskell, and C.A. Johnson (eds.)], Cambridge University Press, Cambridge, United Kingdom and New York, NY, USA, 881pp.

Kaufman, Y.J., D. Tanré, O. Dubovik, A. Karnieli, and L.A. Remer, 2001: Absorption of sunlight by dust as inferred from satellite and ground-based remote sensing. *Geophys. Res. Lett.*, **28**, 1479–1482.

Key, J.R., 2001, *Streamer User's Guide*, Cooperative Institute for Meteorological Satellite Studies, University of Wisconsin, 96 pp.

Kinne, S. and R. Pueschel, 2001: Aerosol radiative forcing for Asian continental outflow. *Atmos. Environ.,* **35**, 5019–5028.

Kubilay, N., T. Cokacar, and T. Oguz, 2003: Optical properties of mineral dust outbreaks over the northeastern Mediterranean. *J. Geophys. Res.*, **108**, 4666, doi:10.1029/2003JD003798.

Li, F., A.M. Vogelmann, and V. Ramanathan, 2004: Saharan dust aerosol radiative forcing measured from space. *J. Climate*, **17**, 2558–2571.

Liao, H. and J.H. Seinfeld, 1998: Radiative forcing by mineral dust aerosols: sensitivity to key variables. *J. Geophys. Res.*, **103**, 31637–31645.

Mikami, M., O. Abe, M. Du, O. Chiba, K. Fujita, M. Hayashi, Y. Iwasaka, K. Kai, K. Masuda, T. Nagai, T. Ootomo, J. Suzuki, A. Uchiyama, S. Yabuki, Y. Yamata, M. Yasui, G. Shi, X. Zhang, Z. Shen, W. Wei, and J. Zhou, 2002: The impact of aeolian dust on climate: Sino-Japanese cooperative project ADEC. *J. Arid Land Studies*, **11**, 211–222.

Miller, R.L. and I. Tegen, 1998: Climate response to soil dust aerosols. *J. Climate*, **11**, 3247–3267.

——— and ———, 1999: Radiative Forcing of a Tropical Direct Circulation by Soil Dust Aerosols. *J. Atmos. Sci.*, **56**, 2403–2433.

Myhre, G. and F. Stordal, 2001: Global sensitivity experiments of the radiative forcing due to mineral aerosols. *J. Geophys. Res.*, **106**, 18193–18204, 10.1029/2000JD900536.

———, A. Grini, J.M. Haywood, F. Stordal, B. Chatenet, D. Tanré, J.K. Sundet, and I.S.A. Isaksen, 2003: Modeling the radiative impact of mineral dust during the Saharan Dust Experiment (SHADE) campaign. *J. Geophys. Res.*, **10**, 8579, doi:10.1029/2002JD002566.

Quijano, A.L., I.N. Sokolik, and O.B. Toon, 2000: Radiative heating rates and direct radiative forcing by mineral dust in cloudy atmospheric conditions. *J. Geophys. Res.*, **105**, 12 207–12 219.

Rothman, L.S., C.P. Rindland, A. Goldman, S.T. Massie, D.P. Edwards, J.-M. Flaud, A. Perrin, C. Camy-Peyret, V. Dana, J.-Y. Mandic, J. Schroeder, A. Mccann, R.R. Gamache, R.B. Wattson, K. Yoshino, K.V. Chance, K.W. Jucks, L.R. Brown, V. Nemtchinov, and P. Varanasi, 1998: The HITRAN molecular spectroscopic database and HAWKS (HITRAN Atmospheric Workstation): 1996 edition. *J. Quant. Spectrosc. Radiat. Transfer*, **60**, 665–710.

Shettle, E.P. and R.W. Fenn, 1979: *Models for the aerosols of the lower atmosphere and the effects of humidity variations on their optical properties*, AFGL-TR-79-0214, Air Force Geophysics Laboratory, 94pp.

Sokolik, I.N. and G. Golitsyn, 1993: Investigation of optical and radiative properties of atmospheric dust aerosols. *Atmos. Environ*., **27A**, 2509–2517.

——— and O.B. Toon. 1996: Direct radiative forcing by anthropogenic airborne mineral aerosols. *Nature*, **381**, 681–683.

——— and ———, 1999: Incorporation of mineralogical composition into models of the radiative properties of mineral aerosol from UV to IR wavelengths. *J. Geophys. Res.,* **104**, 9423–9444.

———, D.M. Winker, G. Bergametti, D.A. Gillette, G. Carmichael, Y.J. Kaufman, L. Gomes, L. Schuetz, and J.E. Penner, 2001: Introduction to special section: Outstanding problems in quantifying the radiative impacts of mineral dust. *J. Geophys. Res.*, **106**, 18015–18027.

Stamnes, K., S.C. Tsay, W. Wiscombe, and K. Jayaweera, 1988: Numerically stable algorithm for discrete-ordinate-method radiative transfer in multiple scattering and emitting layered media. *Appl. Opt.*, **27**, 2502–2509.

Takemura, T., T. Nakajima, O. Dubovik, B.N. Holben, and S. Kinne, 2002: Single-scattering albedo and radiative forcing of various aerosol species with a global three-dimensional model. *J. Climate*, **15**, 333–352.

———, ———, A. Higurashi, S. Ohta, and N. Sugimoto, 2003: Aerosol distributions and radiative forcing over the Asian Pacific region simulated by Spectral Radiation-Transport Model for Aerosol Species (SPRINTARS). *J. Geophys. Res.*, **108**, 8659, doi:10.1029/2002JD003210.

Tanaka, T.Y., K. Orito, T.T. Sekiyama, K. Shibata, and M. Chiba, 2003: MASINGAR, a global tropospheric aerosol chemical transport model coupled with MRI/JMA98 GCM: Model de-

scription. *Pap. Meteorol. Geophys.*, **53**, 119–138.

——— and M. Chiba, 2005: Global simulation of dust aerosol with a chemical transport model, MASINGAR. *J. Meteorol. Soc. Japan*, **83A**, 255–278.

Tanré, D., Y.J. Kaufman, B.N. Holben, B. Chatenet, A. Karnieli, F. Lavenu, L. Blarel, O. Dubovik, L.A. Remer, and A. Smirnov, 2001: Climatology of dust aerosol size distribution and optical properties derived from remotely sensed data in the solar spectrum. *J. Geophys. Res.*, **106**, 18205–18218, 10.1029/2000JD900663.

Tegen, I. and A.A. Lacis, 1996: Modeling of particle size distribution and its influence on the radiative properties of mineral dust aerosol. *J. Geophys. Res.*, **101**, 19 237–19 244.

———, ———, and I. Fung, 1996: The influence on climate forcing of mineral aerosols from disturbed soils. *Nature.*, **380**, 419–422.

Toon, O.B., C.P. McKay, and T.P. Ackerman, 1989: Rapid calculation of radiative heating rates and photodissociation rates in inhomogeneous multiple scattering atmospheres. *J. Geophys. Res.*, **94**, 16287–16301.

Tsay, S.-C., K. Stamnes, and K. Jayaweera, 1989: Radiative energy budget in the cloudy and hazy Arc-tic. *J. Atmos. Sci.*, **46**, 1002–1018.

Wang, H., G. Shi, Te. Aoki, B. Wang, and T. Zhao, 2004: Radiative forcing due to dust aerosol over east Asia-north Pacific region during spring, 2001. *Chinese Science Bulletin*, **49**, 2212–2219.

WMO, 1983: *Report of the Experts Meeting on Aerosols and Their Climatic Effects*, WCP-55, Williamsburg, VA, 28–30 March 1983, 103pp.

Woodward, S., 2001: Modeling the atmospheric life cycle and radiative impact of mineral dust in the Hadley Centre climate model. *J. Geophys. Res.*, **106**, 18,155–18,166.